# Estimation of Partial Carbon Radiation at Each Ionization Stage of $C^{2+}$ to $C^{5+}$ Ions in Large Helical Device*)

Hongming ZHANG[1)], Shigeru MORITA[1,2)], Tetsutarou OISHI[1,2)], Izumi MURAKAMI[1,2)], Xianli HUANG[1)] and Motoshi GOTO[1,2)]

[1)]*Graduate University for Advanced Studies, Toki 509-5292, Japan*
[2)]*National Institute for Fusion Science, Toki 509-5292, Japan*

(Received 27 November 2015 / Accepted 26 January 2016)

Detached plasma has been successfully achieved with use of $m/n$ = 1/1 resonant magnetic perturbation (RMP) coils in a large helical device (LHD) without any additional impurity gas puffing. Study of the impurity radiation is then important to clarify the physical mechanism triggering the RMP-assisted detachment. Resonance lines of CIII (977.02 Å, 2s2p–2s$^2$), CIV (1548.2 Å, 2p–2s), CV (40.27 Å, 1s2p–1s$^2$), and CVI (33.73 Å, 2p–1s) measured by vacuum ultraviolet (VUV) and extreme ultraviolet (EUV) spectrometers are used to estimate the radiation power from $C^{2+}$–$C^{5+}$ ions because carbon is the most abundant impurity element in LHD. For the purpose the spectral intensity from the VUV spectrometer is absolutely calibrated using the EUV spectrometer, with which the spectral intensity has already been calibrated. The partial carbon radiation at each ionization stage of $C^{2+}$ to $C^{5+}$ ions, $P_{\rm rad}(C^{q+})$, can be estimated for attached and detached plasmas by calculating the ratio of the partial carbon radiation to the resonance line based on ADAS atomic code. It is found that the radiation from $C^{3+}$ ions existing near a radial location of $\iota/2\pi = 1$ in the ergodic layer increases up to 40% of the total radiation loss and becomes a dominant origin to trigger the detached plasma, whereas carbon radiation is negligible in the attached plasma.



Keywords: EUV spectroscopy, VUV spectroscopy, detached plasma, radiation loss, carbon radiation

DOI: 10.1585/pfr.11.2402019

## 1. Introduction

Steady operation of detached plasma has been achieved without additional impurity gas puffing in the Large Helical Device (LHD) by forming an $m/n$ = 1/1 magnetic island at $\iota/2\pi = 1$ in the ergodic layer with resonant magnetic perturbation (RMP) coils [1]. Carbon released from graphite divertor plates is a dominant intrinsic impurity in high-density LHD discharges [2]. Then, it seems that the carbon radiation during the plasma detachment is also important for the effective edge plasma cooling triggering the detachment. In LHD, $C^{2+}$ and $C^{3+}$ ions with low ionization energies ($E_{\rm i}$ = 48 and 65 eV) are located near the outer boundary in the ergodic layer, whereas $C^{4+}$ and $C^{5+}$ ions with relatively high ionization energies ($E_{\rm i}$ = 392 and 490 eV) are located near the last closed flux surface (LCFS) [2]. In the RMP-assisted plasma detachment, therefore, it is very interesting to compare the radiation power from $C^{2+}$ and $C^{3+}$ ions located outside $\iota/2\pi = 1$ with that from $C^{4+}$ and $C^{5+}$ ions located inside $\iota/2\pi = 1$.

The partial radiation power at each ionization stage in the carbon ions of $C^{2+}$ to $C^{5+}$, $P_{\rm rad}$ ($C^{q+}$), is analyzed from the line intensities of CIII–CVI resonance transitions, which can be measured with extreme ultraviolet (EUV: 10 - 500 Å) and vacuum ultraviolet (VUV: 300 - 2400 Å) spectrometers. The intensity ratio of $P_{\rm rad}$ ($C^{q+}$) to the resonance line can be used to estimate $P_{\rm rad}$ ($C^{q+}$). For the purpose the electron temperature at the radial location where the carbon ion exists has to be evaluated because the intensity ratio is sensitive to the electron temperature. In addition, the spectral intensity has to be absolutely calibrated for the VUV spectrometer. Thus, the $P_{\rm rad}$ ($C^{q+}$) analyzed with the intensity ratio are compared between attached and detached plasmas.

## 2. Experimental Setup

In LHD, the $m/n$ = 1/1 magnetic island formed by the RMP coil system was originally used for the local island divertor experiment to realize an efficient particle exhaust. The O-point of the $m/n$ = 1/1 magnetic island is then positioned in the outboard side of the horizontally elongated plasma cross section at the #6-O or #7-O toroidal section. In the present study it is called 6-O or 7-O island configuration. Since the detached plasma is realized at the magnetic axis position of $R_{\rm ax}$ = 3.90 m, the $m/n$ = 1/1 island is located in the ergodic layer due to the low edge rotational transform.

The EUV and VUV spectrometers are installed on the #10-O diagnostic port of LHD, as shown in Fig. 1 (a).

*author's e-mail: zhang.hongming@nifs.ac.jp*

*) This article is based on the presentation at the 25th International Toki Conference (ITC25).

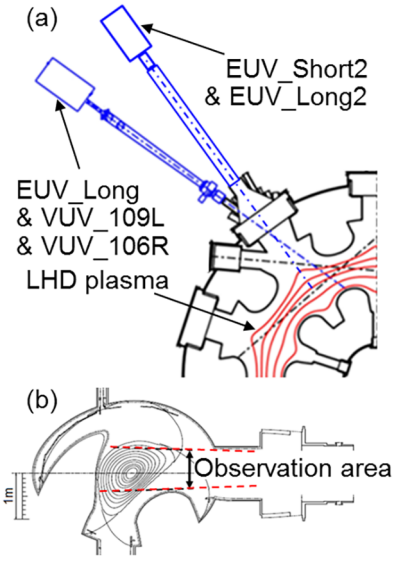


Fig. 1 (a) Schematic view of space-resolved EUV and VUV spectrometers (EUV_Short2 and EUV_Long2) and high-time-resolution EUV and VUV spectrometers (EUV_Long, VUV_109L and VUV_106R) and (b) observation area of EUV_Long, VUV_109L and VUV_106R.

In the present study, two EUV spectrometers named EUV_Short (10 - 100 Å) and EUV_Long (50 - 650 Å) and two 20-cm normal incidence VUV spectrometers named VUV_109L (300 - 1000 Å) and VUV_106R (970 - 1900 Å) are used for simultaneous high-time-resolution measurements (5 ms) of the carbon resonance lines, i.e. CIII (977.02 Å, $2s2p–2s^2$), CIV (1548.2 Å, 2p–2s), CV (40.27 Å, $1s2p–1s^2$) and CVI (33.73 Å, 2p–1s) [3, 4]. Two space-resolved EUV spectrometers named EUV_Short2 and EUV_Long2 are used for simultaneous vertical profile measurements of CIII (386.2 Å), CIV (384.17 Å), CV (40.27 Å) and CVI (33.73 Å) in the range of $-0.6 \leq Z \leq 0.6$ m with a time resolution of 100 ms [5–7]. The EUV_Long, VUV_109L and VUV_106R have a similar observation range, as shown in Fig. 1 (b).

## 3. Calibration of VUV Spectrometers

In order to obtain the absolute intensities of the CIII and CIV resonance lines, the spectral intensity measured by VUV_109L and VUV_106R has to be calibrated into absolute intensity. The wavelength ranges of EUV_Long and VUV_109L overlap between 300 and 650 Å. Because the spectral intensity of EUV_Long has already been calibrated on the basis of the bremsstrahlung profile measurement in previous studies [3, 8], the spectral intensity of VUV_109L can be easily calibrated by directly comparing the same spectrum from both spectrometers in the same wavelength range of 400 - 650 Å. The result is plotted in Fig. 2 with open circles.

In order to calibrate the intensity of the VUV spectra in the long wavelength range, e.g., 650 - 1600 Å, the intensity ratio method is applied. As shown in Fig. 3, two intensity ratios of CIII (977.02 Å/386.2 Å, 2p–2s/3p–2s) and CIV (1548.2 Å/312.4 Å, 2p–2s/3p–2s) are calculated using ADAS atomic code as a function of electron temperature [9]. The contribution of $n_e$ to the ratio can be neglected because the ratio is practically insensitive to $n_e$. Here, the absolute intensities of CIII (386.2 Å) and CIV (312.4 Å) are obtained using the EUV_Long spectrometer.

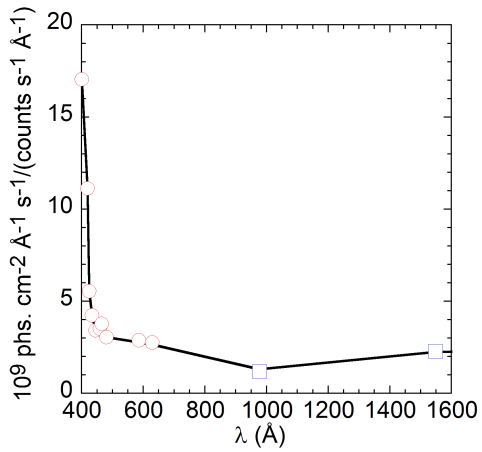


Fig. 2 Absolute intensity calibration factor of VUV_109L and VUV_106R in the wavelength range of 400 - 1600 Å.

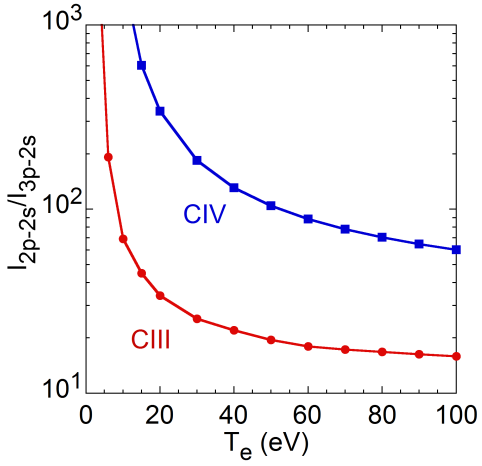


Fig. 3 Intensity ratios of CIII (977.02 Å/386.2 Å) and CIV (1548.2 Å/312.4 Å) calculated with ADAS atomic code.

The electron temperature at the radial location where the $C^{2+}$–$C^{5+}$ ions exist is determined by analyzing the vertical profile of CIII–CVI emissions, as shown in Fig. 4. The vertical profiles of CIII (386.2 Å), CIV (384.02 Å), CV (40.27 Å) and CVI (33.73 Å) are simultaneously observed with EUV_Long2 and EUV_Short2, as shown in Fig. 4 (a). A sharp peak appears in the vertical profile at $0.4 < Z < 0.5$ m because the chord length passing through the edge plasma is long at the top edge in the horizontally elongated plasma cross section. The intensity in CIII–CVI profiles is normalized at each edge peak. Local emissivity pro-

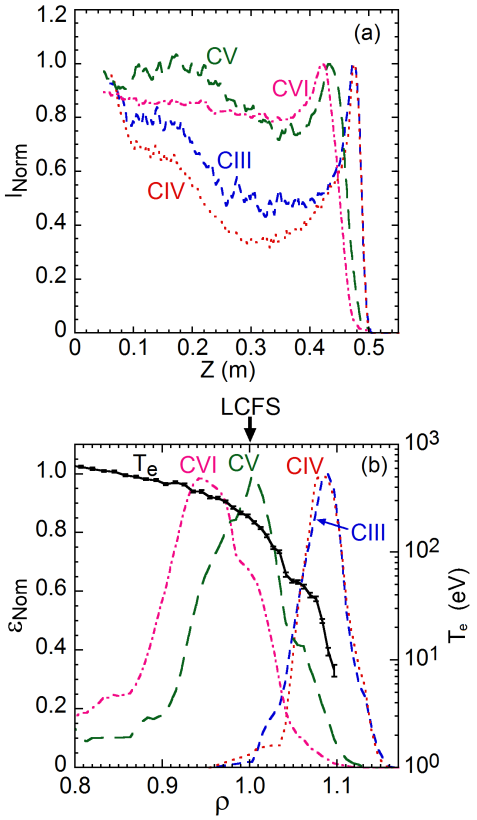


Fig. 4 (a) Normalized chord-integrated vertical profiles of CIII (386.2 Å), CIV (384.02 Å), CV (40.27 Å) and CVI (33.73 Å) and (b) normalized local emissivity profiles of CIII–CVI and $T_e$ profile as a function of minor radius.

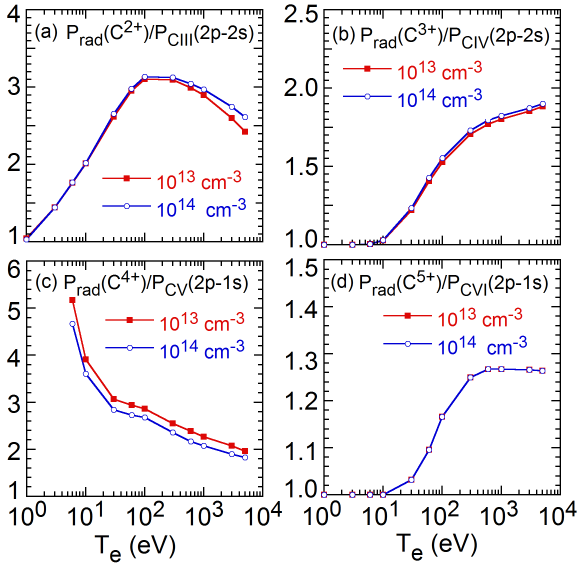


Fig. 5 Ratios of partial carbon radiation power at each ionization stage to radiation power of resonance line calculated with ADAS atomic code: (a) $P_{rad}$ ($C^{2+}$)/$P_{CIII}$ (2p–2s), (b) $P_{rad}$ ($C^{3+}$)/$P_{CIV}$ (2p–2s), (c) $P_{rad}$ ($C^{4+}$)/$P_{CV}$ (2p–1s) and (d) $P_{rad}$ ($C^{5+}$)/$P_{CVI}$ (2p–1s).

files of CIII–CVI are obtained by reconstructing the chord-integrated profiles measured along the vertical direction based on the Abel inversion method. The magnetic surface necessary for the Abel inversion is calculated with the variational moments equilibrium code (VMEC), including the effect of the finite plasma pressure. Although no magnetic surface exists in the ergodic layer, virtual magnetic surfaces are assumed at $\rho > 1$ by extrapolating the magnetic flux surface at $\rho = 1$. This assumption is generally used in LHD when the analysis is carried out for the ergodic layer [6], as shown in Fig. 4 (b). The emissivity profile is also normalized at each peak value. Figure 4 (b) also shows the $T_e$ profile measured by the Thomson scattering system. Then, the electron temperature at radial locations of $C^{2+}$–$C^{5+}$ ions is determined from the peak position in the CIII–CIV emissivity profiles, i.e., 15 eV for $C^{2+}$, 20 eV for $C^{3+}$, 210 eV for $C^{4+}$ and 360 eV for $C^{5+}$.

The intensity ratio in Fig. 3 is determined with the electron temperatures mentioned above. Thus, the spectral intensities from VUV_109L and VUV_106R spectrometers can be absolutely calibrated at wavelengths of 977.02 Å and 1548.2 Å based on the absolute intensities of CIII (386.2 Å) and CIV (312.4 Å) and the intensity ratio. The results obtained from the intensity ratio method are shown in Fig. 2 with open squares. Finally, the analyzed calibration factor is fitted with a smooth curve in the wavelength range of 400 - 1600 Å, as shown in Fig. 2 with solid line.

## 4. Estimation of Partial Radiation $P_{rad}$ ($C^{q+}$)

The radiation power of the resonance transition generally occupies a considerably large part in the radiation power from impurity ions in a certain ionization stage. Because the absolute intensities of the resonance lines of CIII (977.02 Å), CIV (1548.2 Å), CV (40.27 Å) and CVI (33.73 Å) are measured with the EUV and VUV spectrometers, the ratio of $P_{rad}$ ($C^{q+}$) to resonance line intensity in $C^{q+}$ ions can be calculated with the ADAS atomic code. The ratio of $P_{rad}$ ($C^{q+}$) to the resonance line intensity is shown in Figs. 5 (a)-(d) as a function of electron temperature with the parameter of electron density. Because the ratio is practically insensitive to $n_e$, as shown in Fig. 5, the contribution of $n_e$ can be neglected in the present analysis. As the value of $T_e$ for each ionization stage of carbon ions is already determined from the profile analysis done in Fig. 4 (b), $P_{rad}$ ($C^{q+}$) can be evaluated from the intensity ratio in Fig. 5.

## 5. $P_{rad}$ ($C^{q+}$) in Attached and Detached Plasmas

The partial carbon radiation of $P_{rad}$ ($C^{2+}$)–$P_{rad}$ ($C^{5+}$) is analyzed for attached and detached plasmas. Figure 6 shows a comparison of the discharge waveform between attached (Figs. 6 (a)-(f)) and detached (Figs. 6 (g)-(l)) plasmas. These two discharges are operated at the magnetic axis position of $R_{ax}$ = 3.90 m and heated by negative-ion-

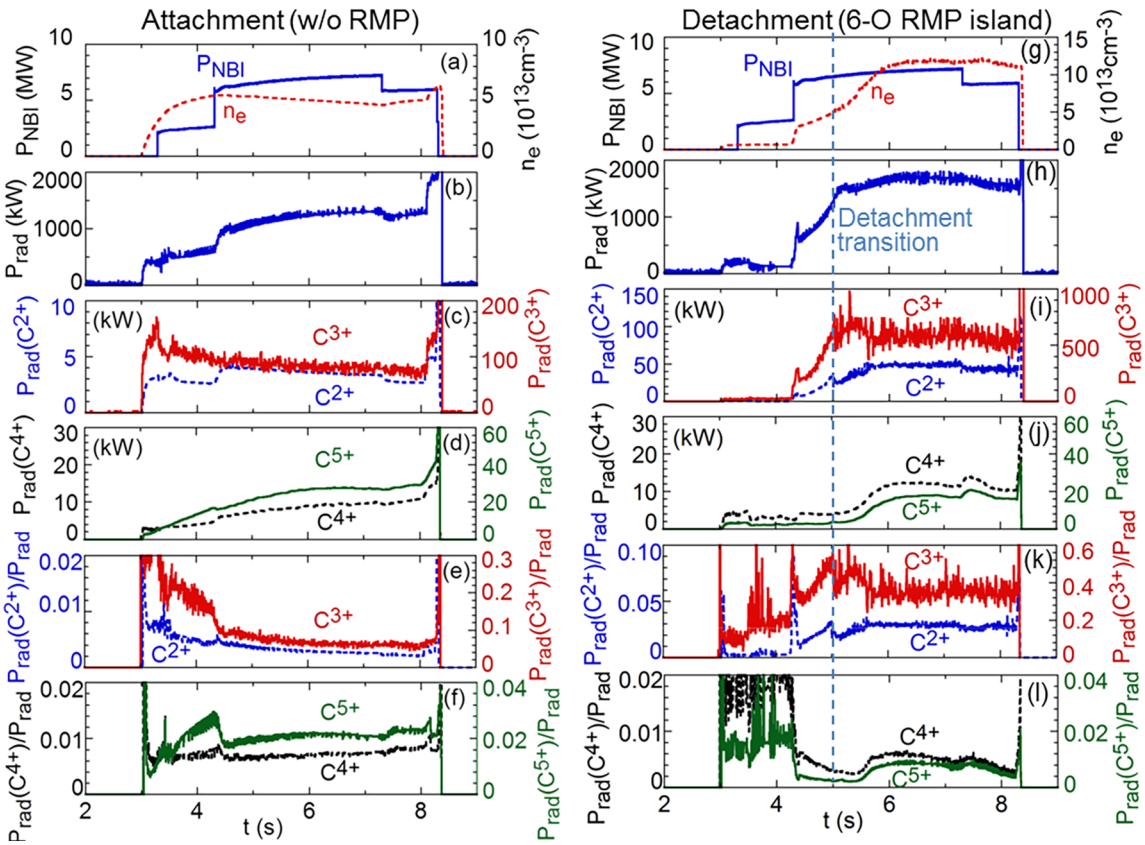


Fig. 6 Time behaviors of (a) NBI port-through power and line-averaged electron density, (b) total radiation loss ($P_{rad}$), partial carbon radiation power of (c) $P_{rad}$ ($C^{2+}$) and $P_{rad}$ ($C^{3+}$) and (d) $P_{rad}$ ($C^{4+}$) and $P_{rad}$ ($C^{5+}$) and ratios of $P_{rad}$ ($C^{q+}$) to $P_{rad}$ of (e) $P_{rad}$ ($C^{2+}$)/$P_{rad}$ and $P_{rad}$ ($C^{3+}$)/$P_{rad}$ and (f) $P_{rad}$ ($C^{4+}$)/$P_{rad}$ and $P_{rad}$ ($C^{5+}$)/$P_{rad}$ in the attached plasma without RMP. Graphs (g)-(l) show the time behaviors for detached plasma with 6-O RMP island in the same meaning as those of graphs (a)-(f).

source-based NBIs. The total radiation loss, $P_{rad}$, shows similar values for both plasmas, i.e., 20% - 25% to the port-through NBI power, $P_{NBI}$. In the attached plasma, the line-averaged electron density is constantly maintained ($\sim 5 \times 10^{13}$ cm$^{-3}$) during $t$ = 4 - 8 s with $P_{rad}$ = 1400 kW. The contributions of $P_{rad}$ ($C^{2+}$) and $P_{rad}$ ($C^{4+}$) to $P_{rad}$ are less than 1%, whereas those of $P_{rad}$ ($C^{3+}$)/$P_{rad}$ and $P_{rad}$ ($C^{5+}$)/$P_{rad}$ are 8% and 2%, respectively.

In the discharge with detached plasma, the $m/n$ = 1/1 island is formed in the ergodic layer and the O-point of the island is located at the outboard side of the #6 toroidal section. With increase in the electron density, plasma detachment occurs at $t$ = 5.0 s, as shown in Figs. 6 (g)-(l). The electron density starts to increase after the occurrence of detachment at $t$ = 5.0 s but saturates at $t$ = 6.0 s. The plasma detachment is steadily maintained at a high density of $n_e$ = $12 \times 10^{13}$ cm$^{-3}$ during $t$ = 6 - 8 s until the end of the NBI pulse. The radiation loss also reaches the maximum value of $P_{rad}$ = 1700 kW during this period. Compared with the attached plasma, it is found that the $P_{rad}$ ($C^{2+}$)/$P_{rad}$ and $P_{rad}$ ($C^{3+}$)/$P_{rad}$ significantly increase to 3% and 40% during the detachment phase, respectively, whereas the increment of $P_{rad}$ is only 300 kW. In contrast, $P_{rad}$ ($C^{4+}$)/$P_{rad}$ and $P_{rad}$ ($C^{5+}$)/$P_{rad}$ do not significantly change compared to the attached plasma.

The drastic increase in $P_{rad}$ ($C^{2+}$) and $P_{rad}$ ($C^{3+}$) during the detachment phase is very clear from the present analysis. $P_{rad}$ ($C^{3+}$) expresses a dominant portion in the total carbon radiation in the detached plasma. A flattening of the $T_e$ profile appears during the detachment phase in edge $T_e$ of 10 - 20 eV at the radial location of the $m/n$ = 1/1 magnetic island [1]. Radial locations of $C^{2+}$ and $C^{3+}$ ions are also broadened reflecting the $T_e$ flattening as shown in Fig. 4 (b). The expansion of the radial location significantly enhances $P_{rad}$ ($C^{2+}$) and $P_{rad}$ ($C^{3+}$) in the detached plasma. Therefore, it is concluded that a change in the edge transport of $C^{2+}$ and $C^{3+}$ ions located near the $m/n$ = 1/1 island brought by the RMP field plays an important role in achieving the present plasma detachment. In addition, the carbon transport near the LCFS is not affected by the supplied RMP field because $P_{rad}$ ($C^{4+}$) and $P_{rad}$ ($C^{5+}$) do not change in both discharges with attachment and detachment.

Before the transition to the detached plasma, the divertor heat flux increases with density, but the edge radiation loss increases much larger than the divertor heat flux. This divertor heat flux level has been usually observed in relatively high-density discharges with attached plasmas. Therefore, the present detachment is certainly triggered by the enhanced edge radiation loss.

# 6. Summary

The partial carbon radiation of $C^{2+}$–$C^{5+}$ ions has been estimated for attached and detached plasmas by analyzing the intensities of the CIII–CVI resonance lines. It is found that the $P_{rad}$ ($C^{3+}$) is much stronger than $P_{rad}$ ($C^{2+}$), $P_{rad}$ ($C^{4+}$) and $P_{rad}$ ($C^{5+}$) in both the attached and detached plasmas. $P_{rad}$ ($C^{3+}$) is much higher in the detached plasma with the 6-O island (40% to $P_{rad}$) compared to that in the attached plasma (8% to $P_{rad}$). $P_{rad}$ ($C^{3+}$) is therefore thought to be the dominant origin for triggering the RMP-assisted detached plasma in LHD.

# Acknowledgements

The authors thank all members of the LHD experimental group for their technical supports. This work was partially carried out under the LHD project financial support (NIFS14ULPP010). This work was also partly supported by the JSPS KAKENHI Grant Number 23340183 and JSPS-NRF-NSFC A3 Foresight Program in the field of Plasma Physics (NSFC: No.11261140328, NRF: No.2012K2A2A6000443).

[1] M. Kobayashi *et al.*, Phys. Plasmas **17**, 056111 (2010).
[2] M.B. Chowdhuri *et al.*, Phys. Plasmas **16**, 062502 (2009).
[3] M.B. Chowdhuri *et al.*, Rev. Sci. Instrum. **78**, 023501 (2007) and Erratum: **84**, 109901 (2013).
[4] T. Oishi *et al.*, Plasma Fusion Res. **10**, 3402031 (2015).
[5] C.F. Dong *et al.*, Rev. Sci. Instrum. **81**, 033107 (2010).
[6] H.M. Zhang *et al.*, Jpn. J. Appl. Phys. **54**, 086101 (2015).
[7] X.L. Huang *et al.*, Rev. Sci. Instrum. **85**, 043511 (2014).
[8] C.F. Dong *et al.*, Rev. Sci. Instrum. **82**, 113102 (2011).
[9] H.P. Summers *et al.*, Plasma Phys. Control. Fusion **48**, 263 (2006).